

Sum-Difference Beamforming for Radar Applications Using Circularly Tapered Random Arrays

Kristopher Buchanan,
John Rockway, and
Oren Sternberg

Electromagnetics and Technology Branch
Code 52260, SSC Pacific
San Diego CA, USA
kris.buchanan@navy.mil

Nam Nicholas Mai
Dept. of Electrical and Computer Engineering,
Johns Hopkins University
Elkridge, MD, USA
nmai1@jhu.edu

Abstract— This work examines a variety of canonical, randomly distributed phased arrays in linear, planar, and volumetric topologies. We investigate their distributed beamforming capabilities in modern mobile autonomous systems. Sum-difference radiation patterns are generated and analyzed for suitability in applications such as amplitude monopulse scanning, direction of arrival estimation, and target tracking. We observe that the inherent randomness of the antenna array distribution alleviates typical half wavelength spacing requirements for grating-lobe free scanning, and tapering of the pattern is accomplished by confining the distribution to quadric topologies. Lastly, comparisons of simulated and measured scanning behavior for conclude the work.

Keywords—Random array, aperiodic array, phased array, ad hoc, wireless networks, collaborative beamforming, cooperative beamforming, distributed beamforming, sensor networks.

I. INTRODUCTION

Multistatic radar systems offer many benefits over classical systems such as irregular scan patterns, power management control, and low side lobe levels, and while they often require complex RF transceiver architectures to achieve these performance capabilities, they can achieve a low probability of intercept (LPI) [1]. Figure 1 shows how a transceiver architecture capable of multiple beam generation can be employed as the front-end for the multistatic system. Another approach to developing such radars is to deploy a distributed sensing network that collectively acts as a phased array [9-12]. If the elements of the network (or array) are coherently connected in phase and time, the array can simultaneously generate beams in arbitrary directions, exploiting the randomness for scanning [4-12].

In this study, we analyze four different topologies for random arrays where we assume the elements are all uniformly distributed: ring random array (RRA), linear random array (LRA), circular random array (CRA), and spherical random array (SRA). These represent the extension as we move from 1 to 3 dimensions. A probabilistic approach is taken to determine mean (expected) performance characteristics as a comparison point for a realized array. We will show that the four distributions above are capable of generating the required sum-

difference (Σ - Δ) beams for monopulse comparison radars, and combined with full scanning ability, we propose the application for use in a monopulse tracking systems (and by extension multistatic).

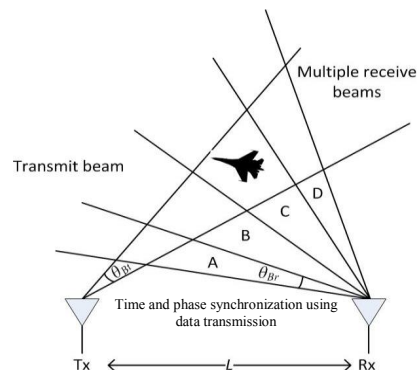


Fig. 1. Multistatic radar configuration from a transceiver system using multiple beams to direction find an airspace.

II. EVEN AND ODD EXPECTED POWER PATTERNS

For completeness, we review the mathematical analysis of random arrays. Consider the array geometry in Figure 2 below, where each black dot indicates the location of an ideal isotropic radiator. The randomness indicates that the radiation pattern is itself a random variable; as such, the analysis proceeds by determining the mean (taking the expected value), where the law of large numbers is assumed. Previous work has extensively shown that this average radiation pattern \bar{U} is [4,8,11-12]

$$\bar{U}(\theta, \phi) = 1/N + (1-1/N) \left| \frac{\Lambda(\zeta_x^r(\theta, \phi)) \Lambda(\zeta_y^r(\theta, \phi))}{\Lambda(\zeta_z^r(\theta))} \right|^2 \quad (1)$$

$$\Lambda = [\text{Main Lobe Factor}] = |\text{Characteristic Function}|^2$$

where the mean radiation pattern \bar{U} is expressed as a sum of a pedestal term, which depends on the number of elements and represents the average sidelobe level, and a product of

characteristic functions. Recall that characteristic functions are simply Fourier transforms of a density function, so the characteristic function describing the net radiation is akin to classical descriptions of beamforming where radiation is determined by the Fourier transform of the aperture [2-3,8]. The functional form of Equation (1) is written using directional cosines for compactness:

$$\begin{aligned}\zeta_x^r(\theta, \phi) &= \hat{x} \cdot \cos(\tilde{\psi}), \zeta_y^r(\theta, \phi) = \hat{y} \cdot \cos(\tilde{\psi}), \tilde{A} = A/\lambda \\ \zeta_z^r(\theta) &= \hat{z} \cdot \cos(\tilde{\psi}), \cos(\tilde{\psi}) = 2\pi\tilde{A}(\hat{r}(\theta, \phi) - \hat{r}(\theta_0, \phi_0))\end{aligned}\quad (2)$$

where A is the measure of aperture radius as in Figure 2.

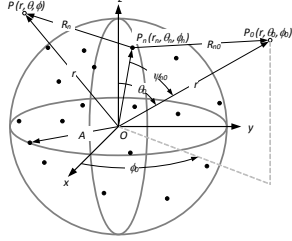


Fig. 2. Geometry of a general 3D random array topology.

In the realization of a generic random array topology, the elements will be bound by some distribution in space, commonly assumed to be either uniform or Gaussian (to obey central limit considerations) [9-12]. Consider now that the spatial distribution is confined to a line, a ring, a planar circle, and a sphere. Assuming that the elements are uniformly distributed in these 4 spatial region, we can write mathematical expressions for the element distributions

$$f_{x,Even}(X) = \frac{(1-x^2)^{(n-1)/2} \Gamma\left[1 + \frac{n}{2}\right]}{\sqrt{\pi} \Gamma\left[\frac{n+1}{2}\right]} \quad (3)$$

$$f_{x,Odd}(X) = \frac{(1-x^2)^{(n-1)/2} \Gamma\left[1 + \frac{n}{2}\right]}{\sqrt{\pi} \Gamma\left[\frac{n+1}{2}\right]} \text{Sgn}(x) \quad (4)$$

where x is used generally as a positional coordinate. Figure 3 shows even and odd mode distribution over a normalized domain of $[-1, 1]$. The n -th order PDF corresponds to a ring ($n = 0$), line ($n = 1$), circle ($n = 2$), and sphere ($n = 3$).

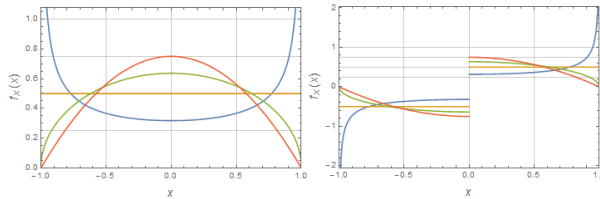


Fig. 3. Distributions of an n -th order random array distribution with (left) even mode and (right) odd mode.

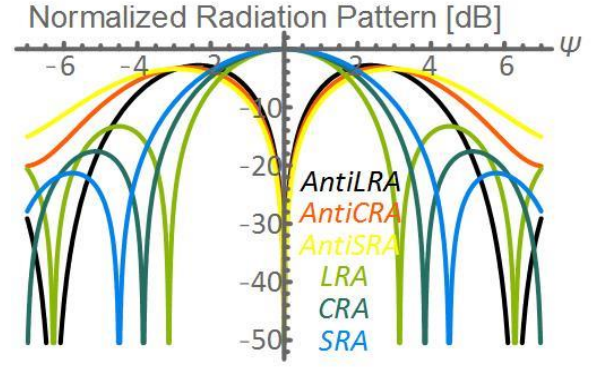


Fig. 4. Sum and difference radiation patterns generated by even and odd modes of a linear (LRA), a circular (CRA), and spherical (SRA) random array.

Applying the distributions above to Equation (1), the generalized expected radiation pattern for an arbitrary array, yields two sets of characteristic functions: an even set for sum beams and an odd set for difference beams

$$\Lambda_{Even}(\Psi) = \text{Sinc}_n(\Psi) = \Gamma(n/2 + 1) J_{n/2}(\Psi) / (\Psi/2)^{n/2} \quad (5)$$

$$\Lambda_{Odd}(\Psi) = \text{CoSinc}_n(\Psi) = \Gamma(n/2 + 1) H_{n/2}(\Psi) / (\Psi/2)^{n/2} \quad (6)$$

For compactness, we use Ψ space defined in Equation (7), since it is well understood in the context of phased array systems; one should note that this is a normalized space so scanning information is lost until Ψ space is brought back to a real coordinate system such as (r, θ, ϕ) .

$$\Psi = \cos^{-1}(kA(\hat{r}(\theta, \phi) - \hat{r}(\theta_0, \phi_0))) \quad (7)$$

Figure 4 shows the normalized radiation patterns for the sum and difference modes clearly generating the beams desired.

Table 1. Even (Sinc) and odd (CoSinc) characteristic functions evaluated for the n -th order topologies (line, ring, planar circle, and sphere).

	$n=0$	$n=1$	$n=2$	$n=3$
$\Lambda_E(\Psi)$	$J_0(\Psi)$	$j_0(\Psi)$	$2J_1(\Psi)/\Psi$	$3j_1(\Psi)/\Psi$
$\Lambda_O(\Psi)$	$jH_0(\Psi)$	$jh_0(\Psi)$	$j2H_1(\Psi)/\Psi$	$j3h_1(\Psi)/\Psi$

Table 1 above enumerates the first few sets of characteristic function solutions for the even and odd modes in Equations (5) and (6). The special functions j_n and h_n are the spherical Bessel and spherical Struve functions, respectively [13-14]. We notice a peculiarity in the solutions for Sinc and CoSinc and observe that they are related by the Hilbert transform. Mathematically, this makes sense as the Hilbert transform represents a 90 degree broadband phase shift, and the Hilbert transform of a sinc is its associated cosinc [15]. As such, we note that we can synthesize the difference mode simply by taking the Hilbert transform of the received sum beams of each circular random array topology. This is a powerful result and can be exploited in modern systems employing digitized frontends.

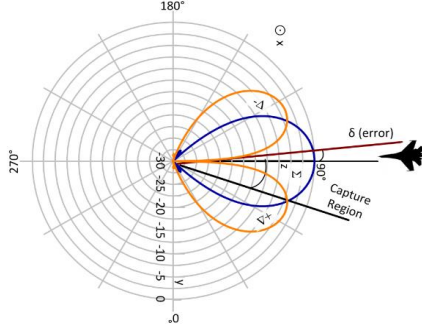


Fig. 5. Angular phase error is found from the ratio of the difference-to-sum voltage ratio.

III. MONOPULSE RADAR SYSTEM

Amplitude comparison monopulse is similar to sequential lobing, but instead, the beams are created simultaneously as shown in Fig. 5. In a tracking system, the sum beam alone (addition of the two beams) is used for transmit, while both sum and difference beams (subtraction of the two beams) are used for receive with the objective of placing the target in the null of the difference pattern in Fig. 5. The sum pattern can be used to range the target, while the difference beam will be used to calculate an angular error [1].

The difference in the amplitudes received from these two beams (the difference beam) gives the angular error, while the angular phase error is found from the ratio of the difference-to-sum voltage ratio

$$e = \frac{\Delta}{\Sigma} = \frac{\text{difference voltage}}{\text{sum voltage}} \quad (8)$$

Applying this concept to the random array topologies above, we see that this would then be given as a ratio of characteristic functions, since they describe the mean pattern behavior of the main beam

$$\frac{\Delta}{\Sigma} = \frac{(\text{CoSinc}_n(\Psi))}{(\text{Sinc}_n(\Psi))} = \frac{(H_{n/2}(\Psi))}{(J_{n/2}(\Psi))} = \text{CoTanc}_n(\Psi) \quad (9)$$

The new function CoTanc is introduced to identify that it is a ratio of two ‘sinc’ type functions (Sinc and CoSinc) from the characteristic functions in Equations (5)-(6). If we isolate the real and imaginary components, we can rewrite the error term as

$$\text{Re} \left\{ \frac{\Delta}{\Sigma} \right\} = \frac{|\Delta|}{|\Sigma|} \cos \delta = |\text{CoTanc}_n \Psi| \cos \delta \quad (10)$$

$$\text{Im} \left\{ \frac{\Delta}{\Sigma} \right\} = \frac{|\Delta|}{|\Sigma|} \sin \delta = |\text{CoTanc}_n \Psi| \sin \delta \quad (11)$$

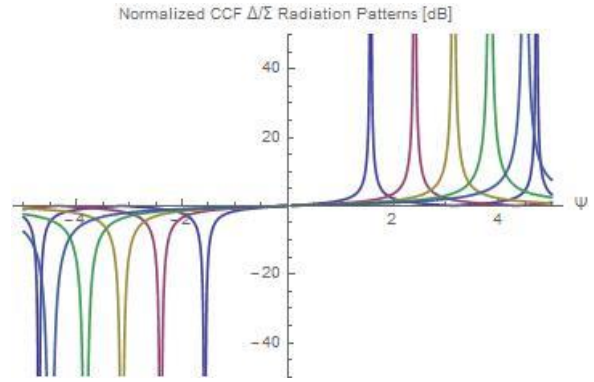


Fig. 6. Comparison of the phase error in Ψ space using analytical equations for the modal beams (Sinc / CoSinc).

where δ is the relative phase between sum and difference beams as in Fig. 5. The common rule of thumb is that the accuracy of a tenth of beam width can be achieved with an SNR of 10 dB [1]. Fig. 6 shows the ambiguity function plotted for each topology. Notice that as the dimension of the topology increases, the ambiguity resolution improves.

As a last point of comparison for the analytical results, we examine the patterns of a line, a ring, a circle, and a sphere on topographical plots where all of the arrays are assumed scanned end fire on the XY plane. Since these are isotropic radiators, there will be no tapering of the back lobe. The Δ/Σ ratios are also given to see how error is given for each topology. Fig. 7 - Fig. 10 show the full beam patterns of the sum and difference modes as well as the associated ambiguity (Tanc and CoTanc).

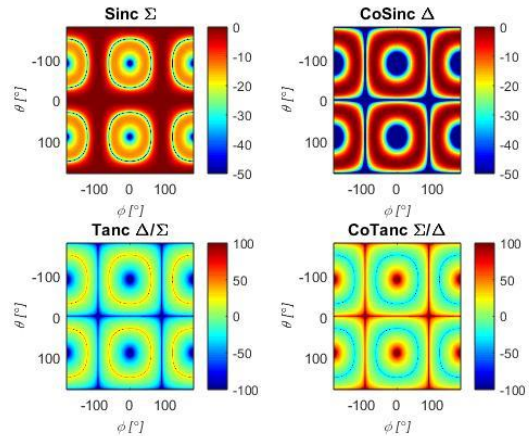


Fig. 7. Full pattern (azimuth and elevation) analysis of a linear random array sum and difference patterns.

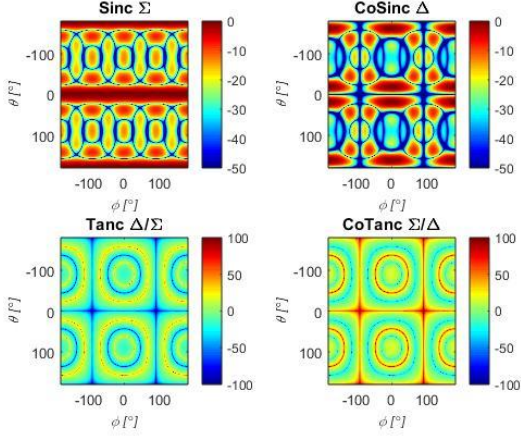


Fig. 8. Full pattern (azimuth and elevation) analysis of a ring random array sum and difference patterns.

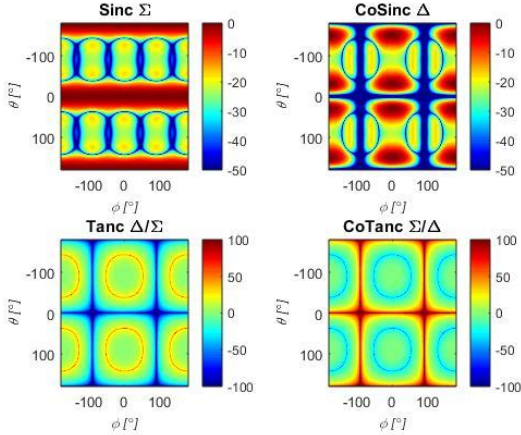


Fig. 9. Full pattern (azimuth and elevation) analysis of a circular random array sum and difference patterns.

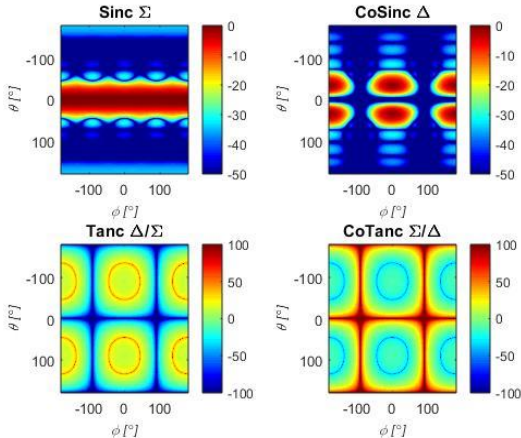


Fig. 10. Full pattern (azimuth and elevation) analysis of a spherical random array sum and difference patterns.

IV. MEASURED PATTERNS AND ANALYSIS

Experimental results were obtained for the linear, ring, circle and sphere random arrays, each confined to a geometry of radius $A = 34$ cm. The antenna elements used in each array are quarter-wave monopoles operating in the 2.4 GHz ISM band, which have an approximately uniform radiation pattern in the azimuth plane. In order to maintain a constant aperture size, the number of elements for each array topology varies due to size constraints on the antennas. Sum and difference beams are generated using the even and odd mode distributions described in Section II. Fig. 11 shows the measured sum and difference beams generated; for the larger apertures such as the sphere and circle, the sidelobe levels are lower due to increasing number of sampling points.

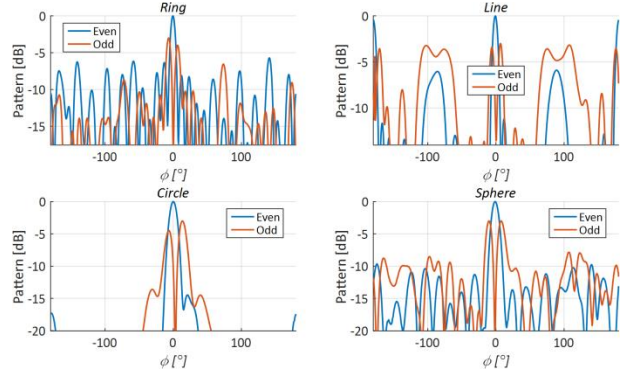


Fig. 11. Measured Sum and difference beams from a linear, ring, circular, and spherical random array.

Using the measured data, we examine the error Δ/Σ in true ϕ space shown in Fig. 12. We observe that the error stays close and bounded to the expected value. Combining this result with the steerability of a circularly symmetric aperture such as a ring, a circle, or sphere, will allow the array to be used in real-time tracking applications since all of the beams can be steered simultaneously instead of requiring a mechanical rotator. This is a powerful result because it will allow for electronic tracking of a target independent of the target's speed.

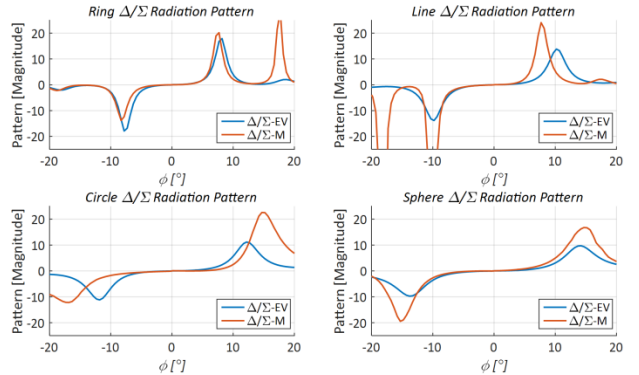


Fig. 12. Δ/Σ phase error generated from the sum and difference beams of the random array.

V. CONCLUSIONS

In this work, we presented the application of sum difference beams from linear, annular, circular, spherical random arrays to monopole radar systems. We showed that even and odd mode symmetries of the array topology can generate the required sum and difference beam, and because of the randomness, a symmetry exists that enable grating-lobe free scanning of the main beam. Analytical and measured data of compare the beam generation and the Δ/Σ error required for monopulse tracking. The results show good agreement between theory and practice.

REFERENCES

- [1] M. I. Skolnik, Radar Handbook, 3rd Edition. McGraw-Hill Companies, New York, NY, 2008.
- [2] A. Bhattacharya, Phased Array Antennas. Hoboken, NJ: John Wiley & Sons, Inc, 2006.
- [3] C. A. Balanis, Antenna Theory: Analysis and Design., 4th ed. New York: John Wiley & Sons, Inc, 2016.
- [4] Y. Lo, "A mathematical theory of antenna arrays with randomly spaced elements," IEEE Trans. Antennas Propag., vol. 12, pp. 257-268, May 1964.
- [5] Y. Lo, "Sidelobe level in nonuniformly spaced antenna arrays," IEEE Antennas Propag., vol. 11, no. 4, pp. 511, 1963.
- [6] Y. Lo, "A probabilistic approach to the design of large antenna arrays," IEEE Trans. Antennas Propag., vol. 11, no. 1, pp. 95-96, 1963.
- [7] A. Panicali and L. Yuen, "A probabilistic approach to large circular and spherical arrays," IEEE Trans. Antennas Propag., vol. 17, pp. 514-522, Jul. 1969.
- [8] B. D. Steinberg, Principles of Aperture & Array System Design, New York: John Wiley & Sons, 1976.
- [9] H. Ochiai, "Collaborative beamforming for distributed wireless ad hoc sensor networks," IEEE Trans. Signal Process., vol. 53, pp. 4110, Nov. 2005.
- [10] M. F. A. Ahmed and S. A. Vorobyov, "Collaborative beamforming for wireless sensor networks with Gaussian distributed sensor nodes," IEEE Trans. on Wireless Commun., vol. 8, pp. 638-643, Feb. 2009.
- [11] K. Buchanan and G. Huff, "A comparison of geometrically bound random arrays in Euclidean space," in IEEE Antennas and Propag. Soc. Int. Symp., Spokane, WA, July 2011, pp. 3-8.
- [12] K. R. Buchanan, "Theory and applications of aperiodic (random) phased arrays," Ph.D. dissertation, Dept. Elect. & Com. Eng., Texas A&M University, TX, 2014.
- [13] F. W. J. Olver, D. W. Lozier, R. F. Boisvert, and C. W. Clark, editors, NIST Handbook of Mathematical Functions, New York: Cambridge Univ. Press, 2010.
- [14] B. McKellar, M. Box and E. Love, "Inversion of the Struve transform of half integer order," J. Austral Math Soc., vol. 25, 1983, pp. 161-174.
- [15] R. Bracewell, The Fourier Transform and Its Applications, 3rd ed. McGraw-Hill Companies, 2000.